

# Large-Scale Gene Network Causal Inference with Bayes Factors of Covariance Structures (BFCS)

Ioan Gabriel Bucur<sup>a,\*</sup>, Tom Claassen<sup>a</sup>, Tom Heskes<sup>a</sup>

<sup>a</sup>*Institute for Computing and Information Sciences, Radboud University, Toernooiveld 212, 6525EC Nijmegen, The Netherlands*

---

## Abstract

Gene regulatory networks play a crucial role in controlling an organism's biological processes, which is why there is significant interest in developing computational methods that are able to extract their structure from high-throughput genetic data. A typical approach consists of a series of conditional independence tests on the covariance structure meant to progressively reduce the space of possible causal models. We propose a novel efficient Bayesian method for discovering the local causal relationships among triplets of (normally distributed) variables. In our approach, we score the patterns in the covariance matrix in one go and we incorporate the available background knowledge in the form of priors over causal structures. Our method is flexible in the sense that it allows for different types of causal structures and assumptions. We apply the approach to the task of inferring gene regulatory networks by learning regulatory relationships between gene expression levels. We show that our algorithm produces stable and conservative posterior probability estimates over local causal structures that can be used to derive an honest ranking of the most meaningful regulatory relationships. We demonstrate the stability and efficacy of our method both on simulated data and on real-world data from an experiment on yeast.

**Keywords:** Causal discovery, Structure learning, Covariance selection, Bayesian inference, Gene regulatory networks

---

## 1. Introduction

Gene regulatory networks (GRNs) play a crucial role in controlling an organism's biological processes, such as cell differentiation and metabolism. If we

---

\*Corresponding author

Email addresses: [g.bucur@cs.ru.nl](mailto:g.bucur@cs.ru.nl) (Ioan Gabriel Bucur), [T.Claassen@science.ru.nl](mailto:T.Claassen@science.ru.nl) (Tom Claassen), [t.heskes@science.ru.nl](mailto:t.heskes@science.ru.nl) (Tom Heskes)

<sup>1</sup>© 2019, Elsevier. Licensed under the Creative Commons Attribution-NonCommercial-NoDerivatives 4.0 International <https://creativecommons.org/licenses/by-nc-nd/4.0/>.

knew the structure of a GRN, we would be able to intervene in the developmental process of the organism, for instance by targeting a specific gene with drugs. In recent years, researchers have developed a number of methods for inferring regulatory relationships from data on gene expression, the process by which genetic instructions are used to synthesize gene products such as proteins. Gene regulatory relationships are inherently causal: we can manipulate the expression level of one gene (the ‘cause’) to regulate that of another gene (the ‘effect’). Because of this, many GRN inference algorithms such as ‘Trigger’ [1], ‘CIT’ [2] or ‘CMST’ [3] are aimed at finding promising causal regulatory relationships among genes.

An efficient way to derive causal relationships from observational data, which results in clear and easily interpretable output, is to find local causal patterns in the data. The *local causal discovery* (LCD) algorithm [4] makes use of a combination of observational data and background knowledge when searching for unconfounded causal relationships among triplets of variables. Trigger is also designed to search for this LCD pattern in the data, using the background knowledge that genetic information is randomized at birth, before any other measurements can be made. Mani et al. [5], on the other hand, divide the causal discovery task into identifying so-called Y structures on subsets of four variables. The Y structure is the smallest pattern containing an unconfounded causal relationship that can be learned solely from observational data in the presence of latent variables.

A key feature of Trigger is that it can estimate the probability of causal regulatory relationships, while controlling for the false discovery rate [1]. The algorithm consists of a series of likelihood ratio tests for regression coefficients that are translated into statements about conditional (in)dependence, which are then used to identify the presence of the LCD pattern. Testing whether regression coefficients are significantly different from zero essentially boils down to testing whether partial correlation coefficients are significantly different from zero [6], which means that all the information needed for the tests lies in the covariance structure.

We propose a Bayesian approach for local causal discovery on triplets of (normally distributed) variables that makes use of the information in the covariance structure. With our method, we directly score patterns in the data by computing posterior probabilities over all possible three-dimensional covariance structures in one go, with the end goal of identifying plausible causal relationships. This provides a stable, efficient and elegant way of expressing the uncertainty in the underlying local causal structure, even in the presence of latent variables. Moreover, it is straightforward to incorporate background knowledge in the form of priors on causal structures. We show how we can plug in our method into an algorithm that searches for local causal patterns in a GRN and outputs a well-calibrated and reliable ranking of the most likely causal regulatory relationships.

The rest of the paper is organized as follows. In Section 2, we introduce some standard background notation and terminology. In Section 3, we describe our Bayesian approach for inferring the covariance pattern of a three-dimensional

Gaussian random vector. By defining simple priors, we then derive the posterior probabilities of local causal structures given the data. In Section 4, we present the results of applying our method on simulated and real-world data. We conclude by discussing advantages and disadvantages of our approach in Section 6.

## 2. Background

Causal structures can be represented by directed graphs, where the nodes in the graph represent (random) variables and the edges between nodes represent causal relationships. *Maximal ancestral graphs* (MAGs) encode conditional independence information and causal relationships in the presence of latent variables and selection bias [7]. We refer to MAGs without undirected edges as *directed maximal ancestral graphs* (DMAGs). DMAGs are closed under marginalization, which means they preserve the conditional independence information in the presence of latent variables.

Two causal structures are *Markov (independence) equivalent* if they imply the same conditional independence statements. The *Markov equivalence class* of a MAG (or DMAG) is represented by a partial ancestral graph (PAG), which displays all the edge marks (arrowhead or tail) shared by all members in the class and displays circles for those marks that are not common among all members. In this work, we will consider two types of graphs: *directed acyclic graphs* and *directed maximal ancestral graphs*. However, the results presented can be applied to any causal graph structure.

A *(conditional) independence model*  $\mathcal{I}$  over a finite set of variables  $V$  is a set of triples  $\langle X, Y \mid Z \rangle$ , called *(conditional) independence statements*, where  $X, Y, Z$  are disjoint subsets of  $V$  and  $Z$  may be empty [8]. We can induce a (probabilistic) independence model over a probability distribution  $P \in \mathcal{P}$  by letting:

$$\langle A, B \mid C \rangle \in \mathcal{I}(P) \iff A \perp\!\!\!\perp B \mid C \text{ w.r.t. } P.$$

The conditional independence model induced by a multivariate Gaussian distribution is a *compositional graphoid* [9], which means that it satisfies the *graphoid axioms* and the *composition* property. Because of this, there is a one-to-one correspondence between the conditional independence models that can be induced by a multivariate Gaussian and the Markov equivalence classes of a causal graph structure.

## 3. Bayes Factors of Covariance Structures (BFCS)

We are interested in inferring the local covariance structure from observational data, assuming the data follows a (latent) Gaussian model. We will be working with triplets of variables. With finite data, we can never be sure about the true covariance structure underlying the data. Hence, we prefer to work

Model	Markov Equivalence Class (PAG)	Covariance Matrix	Precision Matrix
‘ $X_1 \not\perp\!\!\!\perp X_2 \not\perp\!\!\!\perp X_3$ ’ (Full)			
‘ $X_1 \perp\!\!\!\perp X_3$ ’ (Acausal)			
‘ $X_1 \perp\!\!\!\perp X_3 \mid X_2$ ’ (Causal)			
‘ $(X_1, X_3) \perp\!\!\!\perp X_2$ ’ (Independent)			
‘ $X_1 \perp\!\!\!\perp X_2 \perp\!\!\!\perp X_3$ ’ (Empty)			

Figure 1: Overview of the five canonical independence patterns between three variables, depicting the equivalence between causal models, conditional independences, and covariance structures

with probability distributions over covariance matrices. For a general three-dimensional covariance matrix  $\Sigma$ , the likelihood reads:

$$p(\mathbf{D} \mid \Sigma) = (2\pi)^{-\frac{3n}{2}} |\Sigma|^{-\frac{n}{2}} \exp \left[ -\frac{1}{2} \text{tr} (\mathbf{S} \Sigma^{-1}) \right],$$

where  $\mathbf{S} = \mathbf{D}^\top \mathbf{D}$  is the scatter matrix.

Under the Gaussianity assumption, there is a one-to-one correspondence between the constraints in the covariance matrix and the conditional independences among the variables. There are five specific canonical patterns to consider, which are depicted in Figure 1. We show in the appendix that these are the only possible canonical patterns for non-degenerate (full-rank) covariance structures over three variables (1). The ‘full’ and ‘empty’ covariance patterns are self-explanatory. We call ‘independent’ the pattern occurring when one variable is independent of the other two. We call the pattern on the second row ‘acausal’ because  $X_2$  cannot cause  $X_1$  or  $X_3$  if conditioning upon  $X_2$  turns a conditional independence between  $X_1$  and  $X_3$  into a conditional dependence. We call the pattern on the third row ‘causal’ because  $X_2$  either causes  $X_1$  or

$X_3$  if conditioning upon  $X_2$  turns a conditional dependence between  $X_1$  and  $X_3$  into a conditional independence [10]. The five patterns translate into eleven distinct covariance structures when considering all permutations of three variables. These are the only possible covariance structures on three variables, since the conditional independence model induced by a multivariate Gaussian is a compositional graphoid [9].

Our goal is to compute the posterior probability of each of the possible conditional independence models given the data. We denote by  $\mathcal{J} = \{\mathcal{M}_0, \mathcal{M}_1, \dots, \mathcal{M}_{10}\}$  the set of all possible conditional independence models. The model evidence is then, for  $\mathcal{M}_j \in \mathcal{J}$ :

$$p(\mathbf{D} | \mathcal{M}_j) = \int d\mathbf{\Sigma} p(\mathbf{D} | \mathbf{\Sigma}) p(\mathbf{\Sigma} | \mathcal{M}_j).$$

To facilitate computation, we derive the Bayes factors of each conditional independence model ( $\mathcal{M}_j$ ) compared to a reference independence model ( $\mathcal{M}_0$ ):

$$\mathcal{B}_j = \frac{p(\mathbf{D} | \mathcal{M}_j)}{p(\mathbf{D} | \mathcal{M}_0)} = \frac{\int d\mathbf{\Sigma} p(\mathbf{D} | \mathbf{\Sigma}) p(\mathbf{\Sigma} | \mathcal{M}_j)}{\int d\mathbf{\Sigma} p(\mathbf{D} | \mathbf{\Sigma}) p(\mathbf{\Sigma} | \mathcal{M}_0)}.$$

As we shall see in Subsection 3.2, many terms will cancel out, making the resulting ratios much simpler to compute (see for example Equation 5). Finally, we arrive at the posterior probabilities:

$$p(\mathcal{M}_j | \mathbf{D}) = \frac{p(\mathbf{D} | \mathcal{M}_j) \cdot p(\mathcal{M}_j)}{\sum_j p(\mathbf{D} | \mathcal{M}_j) \cdot p(\mathcal{M}_j)} = \frac{\mathcal{B}_j \cdot p(\mathcal{M}_j)}{\sum_j \mathcal{B}_j \cdot p(\mathcal{M}_j)}. \quad (1)$$

### 3.1. Choosing the Prior on Covariance Matrices

We consider the inverse Wishart distribution for three-dimensional covariance matrices, which is parameterized by the positive definite scale matrix  $\mathbf{\Psi}$  and the number of degrees of freedom  $\nu$ :

$$\mathbf{\Sigma} \sim \mathcal{W}_3^{-1}(\mathbf{\Psi}, \nu); \quad p(\mathbf{\Sigma}) = \frac{|\mathbf{\Psi}|^{\frac{\nu}{2}}}{2^{\frac{3\nu}{2}} \Gamma_3(\frac{\nu}{2})} |\mathbf{\Sigma}|^{-\frac{\nu+4}{2}} \exp \left[ -\frac{1}{2} \text{tr}(\mathbf{\Psi} \mathbf{\Sigma}^{-1}) \right].$$

The inverse Wishart is the conjugate prior on the covariance matrix of a multivariate Gaussian vector, which means the posterior is also inverse Wishart. Given the data set  $\mathbf{D}$  containing  $n$  observations and  $\mathbf{S} = \mathbf{D}^T \mathbf{D}$  the scatter matrix, the posterior reads:

$$\mathbf{\Sigma} | \mathbf{D} \sim \mathcal{W}_3^{-1}(\mathbf{\Psi} + \mathbf{S}, \nu + n). \quad (2)$$

In order to choose appropriate parameters for the inverse Wishart prior, we analyze the implied distribution in the space of correlation matrices. By transforming the covariance matrix into a correlation matrix, we end up with a so-called *projected inverse Wishart* distribution on the latter, which we denote by  $\mathcal{PW}^{-1}$ . Barnard et al. have shown that if the correlation matrix  $\mathbf{R}$  follows a projected inverse Wishart distribution with scale parameter  $\mathbf{\Psi}$  and  $\nu$  degrees of

freedom, then the marginal distribution  $p(R_{ij}), i \neq j$ , for off-diagonal elements is uniform if we take  $\Psi$  to be any diagonal matrix and  $\nu = p + 1$ , where  $p$  is the number of variables [11]. We are working with three variables, so we choose  $\nu = 4$ .

It is easy to check that for any diagonal matrix  $D$ , the projected inverse Wishart is scale invariant:

$$\mathcal{PW}^{-1}(\Psi, \nu) \equiv \mathcal{PW}^{-1}(D\Psi D, \nu).$$

From (2), it then follows that we can make the posterior distribution on the correlation matrices independent of the scale of the data by choosing the prior scale matrix  $\Psi = \mathbf{0}_{3,3}$ . Since that would lead to an undefined prior distribution, we can achieve the same goal by setting  $\Psi = \epsilon \mathbf{I}_3$  in the limit  $\epsilon \downarrow 0$ , where  $\mathbf{I}$  is the identity matrix. Summarizing, we will consider the prior distribution:

$$\Sigma \sim \mathcal{W}_3^{-1}(\epsilon \mathbf{I}_3, 4), \quad \epsilon \downarrow 0.$$

### 3.2. Deriving the Bayes Factors

As reference model ( $\mathcal{M}_0$ ), we choose the most general case in which no independences can be found in the data ( $X_1 \not\perp\!\!\!\perp X_2 \not\perp\!\!\!\perp X_3$ ), which means that the covariance matrix is unconstrained (Figure 1, first row). We assume that the covariance matrix follows an inverse Wishart distribution

$$p(\Sigma \mid X_1 \not\perp\!\!\!\perp X_2 \not\perp\!\!\!\perp X_3) = \mathcal{W}_3^{-1}(\Sigma; \epsilon \mathbf{I}_3, \nu),$$

where we consider the limit  $\epsilon \downarrow 0$  and set  $\nu = 4$  (see Subsection 3.1). Using the conjugacy of the inverse Wishart prior for the covariance matrix, we immediately get the model evidence

$$p(\mathbf{D} \mid X_1 \not\perp\!\!\!\perp X_2 \not\perp\!\!\!\perp X_3) = \frac{\epsilon^{\frac{3\nu}{2}} \Gamma_3(\frac{n+\nu}{2})}{\pi^{\frac{3n}{2}} \Gamma_3(\frac{\nu}{2})} |\mathbf{S} + \epsilon \mathbf{I}_3|^{-\frac{n+\nu}{2}}, \quad (3)$$

where  $\Gamma_p$  is the  $p$ -variate gamma function and  $\mathbf{S} = \mathbf{D}^\top \mathbf{D}$  is the scatter matrix.

- We first compare the evidence for the conditional independence model ' $X_1 \perp\!\!\!\perp X_2 \perp\!\!\!\perp X_3$ ' to the evidence for the reference model ' $X_1 \not\perp\!\!\!\perp X_2 \not\perp\!\!\!\perp X_3$ ' by computing the Bayes factor:

$$\mathcal{B}(X_1 \perp\!\!\!\perp X_2 \perp\!\!\!\perp X_3) = \frac{p(\mathbf{D} \mid X_1 \perp\!\!\!\perp X_2 \perp\!\!\!\perp X_3)}{p(\mathbf{D} \mid X_1 \not\perp\!\!\!\perp X_2 \not\perp\!\!\!\perp X_3)}.$$

We can implement the ' $X_1 \perp\!\!\!\perp X_2 \perp\!\!\!\perp X_3$ ' case (Figure 1, last row) by constraining  $\Sigma$  to be diagonal, which means we only have to consider the parameters  $\Sigma_{11}, \Sigma_{22}, \Sigma_{33}$ . We propose to take:

$$p(\Sigma \mid X_1 \perp\!\!\!\perp X_2 \perp\!\!\!\perp X_3) = \prod_{i=1}^3 \mathcal{W}_1^{-1}(\Sigma_{ii}; \epsilon, \nu). \quad (4)$$

The likelihood also factorizes in this case and becomes

$$p(\mathbf{D} \mid \boldsymbol{\Sigma}) = \prod_{i=1}^3 \left\{ (2\pi\Sigma_{ii})^{-\frac{n}{2}} \exp \left[ -\frac{1}{2} \text{tr} (S_{ii}\Sigma_{ii}^{-1}) \right] \right\},$$

yielding the model evidence

$$p(\mathbf{D} \mid X_1 \perp\!\!\!\perp X_2 \perp\!\!\!\perp X_3) = \prod_{i=1}^3 \left[ \frac{\epsilon^{\frac{\nu}{2}} \Gamma_1(\frac{n+\nu}{2})}{\pi^{\frac{n}{2}} \Gamma_1(\frac{\nu}{2})} (S_{ii} + \epsilon)^{-\frac{n+\nu}{2}} \right].$$

Dividing by the model evidence from (3) and taking the limit  $\epsilon \downarrow 0$ , we obtain the Bayes factor

$$\begin{aligned} \mathcal{B}(X_1 \perp\!\!\!\perp X_2 \perp\!\!\!\perp X_3) &= \frac{\Gamma_3(\frac{\nu}{2})}{\Gamma_3(\frac{n+\nu}{2})} \left[ \frac{\Gamma_1(\frac{n+\nu}{2})}{\Gamma_1(\frac{\nu}{2})} \right]^3 |\mathbf{C}|^{\frac{n+\nu}{2}} \\ &= \frac{n+\nu-2}{\nu-2} \frac{\Gamma(\frac{\nu-1}{2})}{\Gamma(\frac{n+\nu}{2})} \frac{\Gamma(\frac{\nu}{2})}{\Gamma(\frac{n+\nu-1}{2})} |\mathbf{C}|^{\frac{n+\nu}{2}}, \end{aligned} \quad (5)$$

with  $\mathbf{C}$  the sample correlation matrix and  $\Gamma$  the (univariate) gamma function. Due to the choice (4), the evidence for ‘ $X_1 \perp\!\!\!\perp X_2 \perp\!\!\!\perp X_3$ ’ also scales with  $\epsilon^{\frac{\nu}{2}}$ , so the dominant terms depending on  $\epsilon$  cancel out and the Bayes factor depends only on the correlation matrix in the limit  $\epsilon \downarrow 0$ .

- We now show how to derive the Bayes factor for the ‘ $X_3 \perp\!\!\!\perp (X_1, X_2)$ ’ case. The derivations for the other two permutations, ‘ $X_1 \perp\!\!\!\perp (X_2, X_3)$ ’ and ‘ $X_2 \perp\!\!\!\perp (X_3, X_1)$ ’, are completely analogous. Given the independence statements, the covariance matrix  $\boldsymbol{\Sigma}$  is block diagonal, consisting of the submatrix  $\boldsymbol{\Sigma}_{(1,2),(1,2)}$  (specified by the parameters  $\Sigma_{11}, \Sigma_{12}, \Sigma_{22}$ ) and the single element  $\Sigma_{33}$ . We thus propose the following prior:

$$p(\boldsymbol{\Sigma} \mid X_3 \perp\!\!\!\perp (X_1, X_2)) = \mathcal{W}_2^{-1}(\boldsymbol{\Sigma}_{(1,2),(1,2)}; \epsilon I_2, \nu) \times \mathcal{W}_1^{-1}(\Sigma_{33}; \epsilon, \nu).$$

The likelihood factorizes accordingly into two terms:

$$\begin{aligned} p(\mathbf{D} \mid \boldsymbol{\Sigma}) &= (2\pi)^{-\frac{2n}{2}} |\boldsymbol{\Sigma}_{(1,2),(1,2)}|^{-\frac{n}{2}} \exp \left[ -\frac{1}{2} \text{tr} \left( \mathbf{S}_{(1,2),(1,2)} \boldsymbol{\Sigma}_{(1,2),(1,2)}^{-1} \right) \right] \times \\ &\quad (2\pi)^{-\frac{n}{2}} \Sigma_{33}^{-\frac{n}{2}} \exp \left[ -\frac{1}{2} S_{33} \Sigma_{33}^{-1} \right]. \end{aligned}$$

The marginal likelihood then reads:

$$p(\mathbf{D} \mid X_3 \perp\!\!\!\perp (X_1, X_2)) = \frac{\epsilon^{\frac{3\nu}{2}}}{\pi^{\frac{3n}{2}}} \frac{\Gamma_1(\frac{n+\nu}{2})}{\Gamma_1(\frac{\nu}{2})} \frac{\Gamma_2(\frac{n+\nu}{2})}{\Gamma_2(\frac{\nu}{2})} (S_{33} + \epsilon)^{-\frac{n+\nu}{2}} |\mathbf{S}_{(1,2),(1,2)} + \epsilon I_2|^{-\frac{n+\nu}{2}}.$$

We obtain the following Bayes factor, in the limit  $\epsilon \downarrow 0$ :

$$\begin{aligned} \mathcal{B}(X_3 \perp\!\!\!\perp (X_1, X_2)) &= \frac{\Gamma_3(\frac{\nu}{2})}{\Gamma_3(\frac{n+\nu}{2})} \frac{\Gamma_2(\frac{n+\nu}{2})}{\Gamma_2(\frac{\nu}{2})} \frac{\Gamma_1(\frac{n+\nu}{2})}{\Gamma_1(\frac{\nu}{2})} \left[ \frac{|\mathbf{C}|}{1 - C_{12}^2} \right]^{\frac{n+\nu}{2}} \\ &= \frac{n+\nu-2}{\nu-2} \left[ \frac{|\mathbf{C}|}{1 - C_{12}^2} \right]^{\frac{n+\nu}{2}}. \end{aligned}$$

- We now show how to derive the Bayes factor for the ‘ $X_1 \perp\!\!\!\perp X_2$ ’ case. The derivations for the other two permutations, ‘ $X_2 \perp\!\!\!\perp X_3$ ’ and ‘ $X_3 \perp\!\!\!\perp X_1$ ’, are completely analogous. The inverse-Wishart distribution factorizes, for arbitrary  $\Psi$  and  $\nu$ , into:

$$\mathcal{W}_3^{-1}(\Sigma; \Psi, \nu) = \mathcal{W}_2^{-1}(\Sigma_{(1,2),(1,2)}; \Psi_{(1,2),(1,2)}, \nu - 1) \times \mathcal{W}_1^{-1}(\Sigma_{33 \cdot (1,2)}; \Psi_{33 \cdot (1,2)}, \nu) \times \mathcal{N}(\Sigma_{(1,2),(1,2)}^{-1} \Sigma_{(1,2),3}; \Psi_{(1,2),(1,2)}^{-1} \Psi_{(1,2),3}, \Sigma_{33 \cdot (1,2)} \Psi_{(1,2),(1,2)}^{-1}).$$

We can implement the constraint  $\Sigma_{12} = 0$  by forcing  $\Sigma_{(1,2),(1,2)}$  to be diagonal. This suggests the prior:

$$p(\Sigma \mid X_1 \perp\!\!\!\perp X_2) = \prod_{i=1}^2 \mathcal{W}_1^{-1}(\Sigma_{ii}; \epsilon, \nu - 1) \times \mathcal{W}_1^{-1}(\Sigma_{33 \cdot (1,2)}; \epsilon, \nu) \times \mathcal{N}(\Sigma_{(1,2),(1,2)}^{-1} \Sigma_{(1,2),3}; 0, \epsilon^{-1} \Sigma_{33 \cdot (1,2)} I_2).$$

Note that in the limit  $\epsilon \downarrow 0$ , the prior normal component moves towards an improper flat distribution:

$$\mathcal{N}(\Sigma_{(1,2),(1,2)}^{-1} \Sigma_{(1,2),3}; 0, \epsilon^{-1} \Sigma_{33 \cdot (1,2)} I_2) \xrightarrow{\epsilon \downarrow 0} \frac{\epsilon}{2\pi \Sigma_{33 \cdot (1,2)}}.$$

In this representation, the likelihood reads:

$$p(\mathbf{D} \mid \Sigma) = \prod_{i=1}^2 (2\pi)^{-\frac{n}{2}} \Sigma_{ii}^{-\frac{n}{2}} \exp \left[ -\frac{1}{2} S_{ii} \Sigma_{ii}^{-1} \right] \times (2\pi)^{-\frac{n}{2}} \Sigma_{33 \cdot (1,2)}^{-\frac{n}{2}} \exp \left[ -\frac{1}{2} S_{33 \cdot (1,2)} \Sigma_{33 \cdot (1,2)}^{-1} \right] \times \mathcal{N}(\Sigma_{(1,2),(1,2)}^{-1} \Sigma_{(1,2),3}; \mathbf{S}_{(1,2),(1,2)}^{-1} \mathbf{S}_{(1,2),3}, \Sigma_{33 \cdot (1,2)} \mathbf{S}_{(1,2),(1,2)}^{-1}) \frac{2\pi \Sigma_{33 \cdot (1,2)}}{|\mathbf{S}_{(1,2),(1,2)}|^{\frac{1}{2}}}.$$

With some bookkeeping, keeping only leading terms in  $\epsilon$ , we obtain:

$$p(\mathbf{D} \mid X_1 \perp\!\!\!\perp X_2) = \frac{\epsilon^{\frac{3\nu}{2}}}{\pi^{\frac{3n}{2}}} \left[ \frac{\Gamma_1(\frac{n+\nu-1}{2})}{\Gamma_1(\frac{\nu-1}{2})} \right]^2 \frac{\Gamma_1(\frac{n+\nu}{2})}{\Gamma_1(\frac{\nu}{2})} S_{11}^{-\frac{n+\nu-1}{2}} S_{22}^{-\frac{n+\nu-1}{2}} S_{33 \cdot (1,2)}^{-\frac{n+\nu}{2}} |\mathbf{S}_{(1,2),(1,2)}|^{-\frac{1}{2}}.$$

Finally, the Bayes factor in the limit  $\epsilon \downarrow 0$  is:

$$\begin{aligned} \mathcal{B}(X_1 \perp\!\!\!\perp X_2) &= \frac{\Gamma_2(\frac{\nu-1}{2})}{\Gamma_2(\frac{n+\nu-1}{2})} \left[ \frac{\Gamma_1(\frac{n+\nu-1}{2})}{\Gamma_1(\frac{\nu-1}{2})} \right]^2 |\mathbf{C}_{(1,2),(1,2)}|^{\frac{n+\nu-1}{2}} \\ &= \frac{\Gamma(\frac{n+\nu-1}{2})}{\Gamma(\frac{n+\nu-2}{2})} \frac{\Gamma(\frac{\nu-2}{2})}{\Gamma(\frac{\nu-1}{2})} (1 - C_{12}^2)^{\frac{n+\nu-1}{2}}. \end{aligned}$$

- We now show how to derive the Bayes factor for the ‘ $X_1 \perp\!\!\!\perp X_2 \mid X_3$ ’ case. The derivation for the other two permutations, ‘ $X_2 \perp\!\!\!\perp X_3 \mid X_1$ ’ and ‘ $X_3 \perp\!\!\!\perp X_1 \mid X_2$ ’, are completely analogous.



is completely analogous. The inverse-Wishart distribution factorizes, for arbitrary  $\Psi$  and  $\nu$ , into:

$$\mathcal{W}_3^{-1}(\Sigma; \Psi, \nu) = \mathcal{W}_2^{-1}(\Sigma_{(1,2),(1,2) \cdot 3}; \Psi_{(1,2),(1,2) \cdot 3}, \nu) \times \mathcal{W}_1^{-1}(\Sigma_{33}; \Psi_{33}, \nu - 2) \times \mathcal{N}(\Sigma_{33}^{-1} \Sigma_{3,(1,2)}; \Psi_{33}^{-1} \Psi_{3,(1,2)}, \Sigma_{(1,2),(1,2) \cdot 3} \Psi_{33}^{-1}).$$

We can implement the constraint  $\Omega_{12} = 0$ , where  $\Omega = \Sigma^{-1}$ , by forcing  $\Sigma_{(1,2),(1,2) \cdot 3}$  to be diagonal. This suggests the prior:

$$p(\Sigma \mid X_1 \perp\!\!\!\perp X_2 \mid X_3) = \prod_{i=1}^2 \mathcal{W}_1^{-1}(\Sigma_{ii \cdot 3}; \epsilon, \nu) \times \mathcal{W}_1^{-1}(\Sigma_{33}; \epsilon, \nu - 2) \times \mathcal{N}(\Sigma_{33}^{-1} \Sigma_{3,(1,2)}; 0, \epsilon^{-1} \Sigma_{(1,2),(1,2) \cdot 3}).$$

where we use the shorthand notation  $\Sigma_{ii \cdot 3}$  to denote  $(\Sigma_{(1,2),(1,2) \cdot 3})_{ii}$  for  $i \in \{1, 2\}$  (same for  $\mathbf{S}$ ). Note that in the limit  $\epsilon \downarrow 0$ , the normal component moves towards an improper flat distribution:

$$\mathcal{N}(\Sigma_{33}^{-1} \Sigma_{3,(1,2)}; 0, \epsilon^{-1} \Sigma_{(1,2),(1,2) \cdot 3}) \xrightarrow{\epsilon \downarrow 0} \frac{\epsilon}{2\pi |\Sigma_{(1,2),(1,2) \cdot 3}|^{\frac{1}{2}}}.$$

In this representation, the likelihood reads:

$$p(\mathbf{D} \mid \Sigma) = \prod_{i=1}^2 (2\pi)^{-\frac{n}{2}} \Sigma_{ii \cdot 3}^{-\frac{n}{2}} \exp \left[ -\frac{1}{2} S_{ii \cdot 3} \Sigma_{ii \cdot 3}^{-1} \right] \times (2\pi)^{-\frac{n}{2}} \Sigma_{33}^{-\frac{n}{2}} \exp \left[ -\frac{1}{2} S_{33} \Sigma_{33}^{-1} \right] \times \mathcal{N}(\Sigma_{33}^{-1} \Sigma_{3,(1,2)}; S_{33}^{-1} \mathbf{S}_{3,(1,2)}, \Sigma_{(1,2),(1,2) \cdot 3} S_{33}^{-1}) \frac{2\pi |\Sigma_{(1,2),(1,2) \cdot 3}|^{\frac{1}{2}}}{S_{33}}.$$

With some bookkeeping, keeping only leading terms in  $\epsilon$ , we obtain:

$$p(\mathbf{D} \mid X_1 \perp\!\!\!\perp X_2 \mid X_3) = \frac{\epsilon^{\frac{3\nu}{2}}}{\pi^{\frac{3n}{2}}} \left[ \frac{\Gamma_1(\frac{n+\nu}{2})}{\Gamma_1(\frac{\nu}{2})} \right]^2 \frac{\Gamma_1(\frac{n+\nu-2}{2})}{\Gamma_1(\frac{\nu-2}{2})} S_{11 \cdot 3}^{-\frac{n+\nu}{2}} S_{22 \cdot 3}^{-\frac{n+\nu}{2}} S_{33}^{-\frac{n+\nu}{2}}.$$

Finally, the Bayes factor in the limit  $\epsilon \downarrow 0$  is:

$$\begin{aligned} \mathcal{B}(X_1 \perp\!\!\!\perp X_2 \mid X_3) &= \frac{\Gamma_2(\frac{\nu}{2})}{\Gamma_2(\frac{n+\nu}{2})} \left[ \frac{\Gamma_1(\frac{n+\nu}{2})}{\Gamma_1(\frac{\nu}{2})} \right]^2 \left[ \frac{|\mathbf{C}_{(1,2),(1,2) \cdot 3}|}{C_{11 \cdot 3} C_{22 \cdot 3}} \right]^{\frac{n+\nu}{2}} \\ &= \frac{\Gamma(\frac{n+\nu}{2})}{\Gamma(\frac{n+\nu-1}{2})} \frac{\Gamma(\frac{\nu-1}{2})}{\Gamma(\frac{\nu}{2})} \left[ \frac{|\mathbf{C}|}{(1 - C_{13}^2)(1 - C_{23}^2)} \right]^{\frac{n+\nu}{2}}. \end{aligned}$$

In conclusion, we obtain the *Bayes factors on covariance structures* (BFCS):

$$\begin{aligned}
\mathcal{B}(X_1 \perp\!\!\!\perp X_2 \perp\!\!\!\perp X_3) &= f(n, \nu) g(n, \nu) |\mathbf{C}|^{\frac{n+\nu}{2}} \\
\mathcal{B}(X_3 \perp\!\!\!\perp (X_1, X_2)) &= f(n, \nu) \left( \frac{|\mathbf{C}|}{1 - C_{12}^2} \right)^{\frac{n+\nu}{2}} \\
\mathcal{B}(X_1 \perp\!\!\!\perp X_2 \mid X_3) &= g(n, \nu) \left( \frac{|\mathbf{C}|}{(1 - C_{13}^2)(1 - C_{23}^2)} \right)^{\frac{n+\nu}{2}} \\
\mathcal{B}(X_1 \perp\!\!\!\perp X_2) &= \frac{f(n, \nu)}{g(n, \nu)} (1 - C_{12}^2)^{\frac{n+\nu-1}{2}},
\end{aligned} \tag{6}$$

where  $f(n, \nu) = \frac{n + \nu - 2}{\nu - 2}$  and  $g(n, \nu) = \frac{\Gamma(\frac{n+\nu}{2}) \Gamma(\frac{\nu-1}{2})}{\Gamma(\frac{n+\nu-1}{2}) \Gamma(\frac{\nu}{2})} \approx \left( \frac{2n + 2\nu - 3}{2\nu - 3} \right)^{\frac{1}{2}}$ .

For deriving the Bayes factors in (6), we only need to plug in the correlation matrix with the number of samples and compute a limited number of closed-form terms. This is then sufficient to obtain the full posterior distribution over the covariance structures, which makes the BFCS method fast and efficient.

### 3.3. Priors on Causal Structures

To do a full Bayesian analysis, we need to specify priors over the different conditional independence models. Assuming faithfulness, there is a one-to-one correspondence between the Markov equivalence classes of the underlying causal graph structure and the conditional independence models. By taking a uniform prior over causal graphs and denoting by  $|\mathcal{M}_j|$  the number of causal graphs consistent with the independence model  $\mathcal{M}_j \in \mathcal{J}$ , we arrive at the prior:

$$p(\mathcal{M}_j) = \frac{|\mathcal{M}_j|}{\sum_j |\mathcal{M}_j|}, \quad \forall \mathcal{M}_j \in \mathcal{J}.$$

Pattern	CI Model	Description	DAG	DAG w/ BK	DMAG	DMAG w/ BK
Full	$\mathcal{M}_0$	$X_1 \not\perp\!\!\!\perp X_2 \not\perp\!\!\!\perp X_3$	6	2	19	3
Acausal	$\mathcal{M}_1$	$X_1 \perp\!\!\!\perp X_2$	1	1	3	2
	$\mathcal{M}_2$	$X_2 \perp\!\!\!\perp X_3$	1	0	3	0
	$\mathcal{M}_3$	$X_3 \perp\!\!\!\perp X_1$	1	1	3	2
Causal	$\mathcal{M}_4$	$X_1 \perp\!\!\!\perp X_2 \mid X_3$	3	1	5	1
	$\mathcal{M}_5$	$X_2 \perp\!\!\!\perp X_3 \mid X_1$	3	1	5	1
	$\mathcal{M}_6$	$X_3 \perp\!\!\!\perp X_1 \mid X_2$	3	1	5	1
Independent	$\mathcal{M}_7$	$X_1 \perp\!\!\!\perp (X_2, X_3)$	2	2	3	3
	$\mathcal{M}_8$	$X_2 \perp\!\!\!\perp (X_3, X_1)$	2	1	3	1
	$\mathcal{M}_9$	$X_3 \perp\!\!\!\perp (X_1, X_2)$	2	1	3	1
Empty	$\mathcal{M}_{10}$	$X_1 \perp\!\!\!\perp X_2 \perp\!\!\!\perp X_3$	1	1	1	1
All			25	12	53	16

Table 1: Number of causal graph structures over three variables in each Markov equivalence class. In the columns marked ‘w /BK’, the background knowledge that  $X_1$  precedes all other variables, i.e., there can be no arrowhead towards  $X_1$ , is added when counting the number of structures.

In Table 1 we count the number of DAGs and DMAGs (see Section 2) consistent with each covariance pattern (see Figure 1). For example, if we assume

an underlying DAG structure, then  $p(X_1 \perp\!\!\!\perp X_2 \perp\!\!\!\perp X_3) = \frac{1}{25}$ . The addition of background knowledge (BK) reduces the number of causal graph structures corresponding to each conditional independence model. Specifically relevant for discovering causal regulatory relationships is the background knowledge that the genetic marker precedes the expression traits, i.e., that  $X_1$  precedes all other variables. This additional constraint leads to the counts in the columns marked ‘w/ BK’ in Table 1. Some of the covariance patterns imply acausal / causal statements (Figure 1), which is what allows us to directly translate the posterior probabilities over covariance patterns into statements over causal relationships.

Now that we have defined priors on the conditional independence models (Markov equivalence classes), we can derive the posterior probabilities from equations (1) and (6). We are mainly interested in finding the causal structure  $X_1 \rightarrow X_2 \rightarrow X_3$ , which corresponds to the LCD pattern [4]. Assuming DAGs or DMAGs with the background knowledge that  $X_1$  precedes all other variables, there is a one-to-one correspondence between the causal structure and the conditional independence model  $\mathcal{M}_6$ , so we want to estimate  $p(\mathcal{M}_6 | \mathbf{D})$ .

For each prior, we can compute a different upper bound on the probability  $p(\mathcal{M}_6 | \mathbf{D})$ , which represents a limit on the confidence in this statement given a particular number of samples. From Equation (1), this upper bound is given by

$$p(\mathcal{M}_6 | \mathbf{D}) = \frac{\mathcal{B}(X_3 \perp\!\!\!\perp X_1 | X_2) \cdot p(X_3 \perp\!\!\!\perp X_1 | X_2)}{\sum_{i=0}^{10} \mathcal{B}(\mathcal{M}_i) \cdot p(\mathcal{M}_i)} \leq \frac{\mathcal{B}(\mathcal{M}_6) \cdot p(\mathcal{M}_6)}{\mathcal{B}(\mathcal{M}_6) \cdot p(\mathcal{M}_6) + p(\mathcal{M}_0)}.$$

Furthermore, we have that for any correlation matrix  $\mathbf{C}$ :

$$|\mathbf{C}| = 1 + 2C_{12}C_{13}C_{23} - C_{12}^2 - C_{13}^2 - C_{23}^2 \leq (1 - C_{12}^2)(1 - C_{13}^2).$$

It is easy to show that this inequality is equivalent to  $(C_{12}C_{23} - C_{13})^2 \geq 0$ . Combining this result with the Bayes factor expression for  $\mathcal{M}_6$  in (6), we get  $\mathcal{B}(\mathcal{M}_6) \leq g(n, \nu)$ , which in turn implies:

$$p(\mathcal{M}_6 | \mathbf{D}) \leq \frac{\mathcal{B}(\mathcal{M}_6) \cdot p(\mathcal{M}_6)}{\mathcal{B}(\mathcal{M}_6) \cdot p(\mathcal{M}_6) + p(\mathcal{M}_0)} \leq \frac{g(n, \nu) \cdot p(\mathcal{M}_6)}{g(n, \nu) \cdot p(\mathcal{M}_6) + p(\mathcal{M}_0)}. \quad (7)$$

This result means that the posterior probability of ‘ $X_1 \perp\!\!\!\perp X_3 | X_2$ ’ that can be derived is upper bounded by a quantity that depends on the number of observations and on the prior belief in ‘ $X_1 \perp\!\!\!\perp X_3 | X_2$ ’ versus the full model.

The posterior probabilities could also be derived by combining the Bayesian Gaussian equivalent (BGe) score [12] with the priors on causal structures defined in this subsection. Due to our choice of priors on covariance matrices (see Subsection 3.1), however, the Bayes factors are simpler to compute. This makes our approach more efficient when used to infer causal relationships in large regulatory networks.

To summarize, we have developed a method for computing the posterior probabilities of the covariance structures over three variables (BFCS). We will employ this procedure as part of an algorithm for discovering regulatory relationships. Similarly to LCD and Trigger, the idea is to search over triplets of variables to find potential local causal structures (see Algorithm 1).

### 3.4. Finding Causal Links Using BFCS

Now that we have derived the posterior probability of the causal structure  $p(X_1 \rightarrow X_2 \rightarrow X_3 | \mathbf{D})$ , we would like to estimate the probability of the causal link  $X_2 \rightarrow X_3$ . There are multiple ways of arriving at an estimate of this link. In Trigger, this is handled by limiting the search to the variable  $X_1$  that has the (locally) strongest primary linkage to  $X_2$  and then using the estimate for  $p(X_1 \rightarrow X_2 \rightarrow X_3 | \mathbf{D})$  as the posterior probability of the causal link. This selection strategy will reduce the search space significantly, but it does not necessarily lead to the best estimate, because the variable with the strongest primary linkage might also be linked to  $X_3$ . Instead, we propose to derive the posterior probability of  $X_k \rightarrow X_2 \rightarrow X_3$  given the data for each available  $X_k$  with our much more efficient approach and take the maximum of these probabilities over  $k$ . Similarly to the authors of Trigger, we report this value as a conservative estimate for the probability of  $X_2 \rightarrow X_3 | \mathbf{D}$ . In conclusion, we not only have a different way of estimating the posterior probabilities of causal structures, but we also employ a different search strategy when translating these into the probability of a causal link.

## 4. Experimental Results

### 4.1. Consistency of Detecting Local Causal Structures

In this simulation, we assessed how well our BFCS approach is able to detect the causal structure  $X_1 \rightarrow X_2 \rightarrow X_3$ , which is crucial to the application of the LCD and Trigger algorithms. We considered the three generating structures depicted in Figure 2. In all three cases, the variables are mutually marginally dependent, but only in the first model  $X_1 \perp\!\!\!\perp X_3 | X_2$  holds.

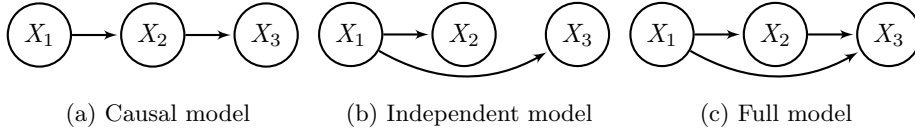


Figure 2: Generating models

We sampled random structural parameters (interaction strengths) for each causal relationship from independent standard normal distributions. Then, given each generating model, we generated data sets of different sizes (from  $10^2$  up to  $10^6$  samples). For each data set, we computed the correlation matrix, which we plugged into 6 for computing the Bayes factors. We repeated this procedure for 1000 different parameter configurations. We assumed that  $X_1$  precedes all other variables and we allowed for latent variables, so we did not use the knowledge that the data is causally sufficient. We considered a uniform prior over the twelve possible DMAG structures (see Table 1).

In the first experiment we generated random multivariate data from the models in Figure 2. As expected, the posterior probability  $p(X_1 \rightarrow X_2 \rightarrow X_3 | \mathbf{D})$

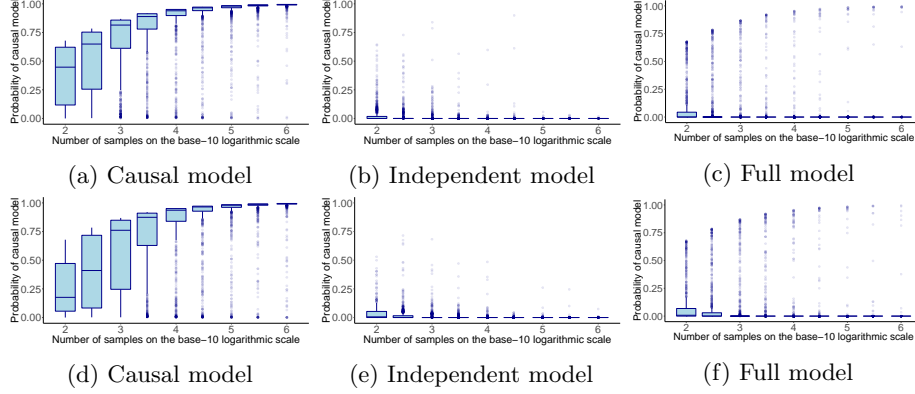


Figure 3: Box plots of the posterior probabilities of  $p(X_1 \rightarrow X_2 \rightarrow X_3 | \mathbf{D})$  output by BFCS across the 1000 different parameter configurations for each of the generating models in Figure 2. As we increased the number of samples, the probability  $p(X_1 \rightarrow X_2 \rightarrow X_3 | \mathbf{D})$  converged to one when the data was generated from the causal model (a) and converged to zero when it was not (b and c). **Top:**  $\mathbf{x} = (X_1, X_2, X_3)$  is multivariate Gaussian; **Bottom:**  $X_1$  is Bernoulli and  $(X_2, X_3) | X_1$  is Gaussian.

converged to one (Figure 3, top row) when the true generating model was the one in Figure 2a. At the same time,  $p(X_1 \rightarrow X_2 \rightarrow X_3 | \mathbf{D})$  converged to zero when the true generating model was the independent or full model. Note that it is easier to distinguish the causal model from the independent model than from the full model. When generating data from the full model, it is possible to generate structural parameters that are close to zero. If the direct interaction between  $X_1$  and  $X_3$  is close to zero, it looks as if  $X_1 \perp\!\!\!\perp X_3 | X_2$ .

In the second experiment, we considered the same generating models, but we sampled  $X_1$  from a Bernoulli distribution to mimic a genetic variable, e.g., an allele or the parental strain in the yeast experiment [1]. We sampled a different success probability for the Bernoulli variable in each repetition from a uniform distribution between 0.1 and 0.9. The random vector  $(X_2, X_3)$  was sampled from a bivariate Gaussian conditional on the value of  $X_1$ . In the bottom row of Figure 3 we see that when the Gaussian assumption did not hold for  $X_1$ , we lost some power in recovering the correct model. When we increased the number of samples, this loss in power due to the violation of the Gaussian assumption became less severe and BFCS remained consistent.

#### 4.2. Causal Discovery in Gene Regulatory Networks

In this series of experiments, we simulated transcriptional regulatory networks meant to emulate the yeast data set analyzed in [1]. We randomly generated data for 100 genetic markers, where each marker is an independent Bernoulli variable with ‘success’ probability uniformly sampled between 0.1 and 0.5. We then generated transcript level expression data from the structural equation model (SEM):

$$\mathbf{t} := \mathbf{B}\mathbf{t} + \mathbf{A}\mathbf{l} + \boldsymbol{\varepsilon},$$

where  $\mathbf{t} = (T_1, T_2, \dots, T_{100})^\top$  is the random vector of the expression trait data,  $\mathbf{l} = (L_1, L_2, \dots, L_{100})^\top$  is the random vector of the genetic markers,  $\mathbf{B}$  is a lower triangular matrix describing the regulatory network structure,  $\mathbf{A}$  is the matrix describing the causal links between the genetic markers and the expression traits, and  $\varepsilon \sim \mathcal{N}(\mathbf{0}_{100}, \mathbf{I}_{100})$  is added noise.

The true causal relationships between gene expression levels are encoded in the directed graph structure defined by  $\mathbf{B}$ , which has been randomly generated using the `randomDAG` function from the R `pcalg` package [13]. In the yeast data set each genetic marker is on average linked to 5.79 expression traits, where we used an absolute correlation coefficient threshold of 0.5 to define ‘linked’, so we randomly sampled the non-zero terms of  $\mathbf{A}$  from a binomial distribution with 0.05 success probability. The strengths of the non-zero terms in  $\mathbf{A}$  and  $\mathbf{B}$  were sampled from a  $\mathcal{U}(-1, 1)$  distribution. We generated data from two simulated gene regulatory networks on 100 expression traits, given 100 genetic markers: one sparser (54 directed edges) and one denser (247 directed edges).

We evaluated the performance of BFCS in terms of the Receiving Operating Characteristic (ROC), Precision-Recall (PRC), and calibration curves. We included three versions of the approach in the comparison. In the first two versions, we take the maximum over all probability estimates of  $\hat{p}(L_k \rightarrow T_i \rightarrow T_j \mid \mathbf{D})$  as our conservative estimate for  $p(T_i \rightarrow T_j \mid \mathbf{D})$ . The only difference between these two versions is in the prior on causal structures: a uniform prior on DAGs (‘BFCS DAG’) and DMAGs (‘BFCS DMAG’), respectively, both incorporating the background knowledge that  $L_k$  cannot be caused by  $T_i$  or  $T_j$ . In the third version of BFCS (‘BFCS loclink’), we first used the selection strategy of Trigger (implemented as `trigger.loclink` in [14]) to choose a candidate genetic marker  $L_i$  exhibiting the strongest primary linkage to  $T_i$  among all available genetic markers. We then used BFCS to estimate  $\hat{p}(L_i \rightarrow T_i \rightarrow T_j \mid \mathbf{D})$  and reported this quantity as our conservative estimate for  $p(T_i \rightarrow T_j \mid \mathbf{D})$ . As a reference, we included an equivalent method based on the ‘Bayesian Gaussian equivalent’ (BGe) score in the comparison, for which we used the same prior on causal structures as ‘BFCS DMAG’. To ensure a fairer comparison, we scaled and centered the data sets generated from the GRNs before computing the BGe score, since BFCS does not make use of any information regarding the location or scale of the data.

We first evaluated how well the algorithms under comparison perform in detecting direct causal regulatory relationships, i.e., those corresponding precisely to the directed edges in the generating network structure (Figures 4 and 5). All methods performed better when the underlying network structure was sparser, since there are fewer connections in the graph that can lead to conditional independences resulting from path cancellations. When comparing BFCS to Trigger, we see that all BFCS versions show an improvement in the AUC measure for the ROC and precision-recall curves, in particular ‘BFCS DAG’ and ‘BFCS DMAG’. We obtained a significantly higher precision for the first causal relationships that are recalled, especially when the data sample size was lower. This suggests that BFCS is better at ranking the top causal regulatory relationships (see also Subsection 4.3). All BFCS versions, in particular ‘BFCS loclink’ are

also better calibrated than Trigger. However, it is important to note that both the BFCS and Trigger approaches are calibrated on detecting the local causal structure  $L_k \rightarrow T_i \rightarrow T_j$ , not on finding the causal link  $T_i \rightarrow T_j$ . Trigger in particular lies well under the diagonal line, indicating that its estimated probabilities are consistently overly optimistic. The BGe reference method performs similarly to BFCS in terms of ROC and PRC, but is less well calibrated.

We noticed that ‘BFCS loclink’, which employs the same genetic marker search strategy as Trigger for deriving the probability of a causal link given the data, performs better than the other two BFCS versions in terms of calibration, but worse in terms of ROC and PRC. When computing the maximum over posterior probability estimates for many local causal structures, like in ‘BFCS DAG’ and ‘BFCS DMAG’, we expected that the calibration will deteriorate. The more causal structures we look at, the higher the chance that we will accidentally find a triple where the conditional independence we are searching for approximately holds. However, it is still unlikely that we will get a very high probability estimate for this ‘accidental’ conditional independence, which is why the calibration is mainly affected in the bins where these estimates are smaller. At the same time, by considering all triples, we increase the chances of finding a relevant genetic marker for which  $L_k \rightarrow T_i \rightarrow T_j$  is the true local causal structure. The estimates for these triples be relatively high, so we will obtain a significant boost in precision for the causal links with the highest estimated posterior probabilities.

Even though we may be mostly interested in direct causal regulatory relationships, the BFCS and Trigger approaches are designed to look for a conditional independence  $L_k \perp\!\!\!\perp T_j \mid T_i$ , which may mean a direct link from  $T_i$  to  $T_j$  or a causal (regulatory) chain comprised of more than two variables (expression traits). Nevertheless, it would be straightforward to perform a subsequent mediation analysis in order to distinguish between direct and indirect causal links. Since BFCS and Trigger are able to pick up ancestral (direct or indirect) causal links, it behooves us to (also) use the transitive closure of the network structure as the gold standard against which to evaluate these methods. When looking at ancestral causal regulatory relationships, all algorithms show an improvement in calibration (Figure 6 compared to Figure 4 and Figure 7 compared to Figure 5), but also a deterioration in the AUC of ROC and PRC. Despite the fact that more causal relationships picked up by the inference algorithms are now labeled as correct, there are also many more relations to be discovered: 73 ancestral versus 51 direct for the sparser network and 970 ancestral versus 225 direct for the denser network.

### 4.3. Comparing Results from an Experiment on Yeast

Chen et al. showcased the Trigger algorithm in [1] by applying it to an experiment on yeast, in which two distinct strains were crossed to produce 112 independent recombinant segregant lines. Genome-wide genotyping and expression profiling were performed on each segregant line. We computed the probabilities over the triples in the yeast data set using `trigger` [14] and BFCS

---

**Algorithm 1** Running BFCS on the yeast data set

---

- 1: *Input:* Yeast data set consisting of 3244 markers and 6216 gene expression measurements
  - 2: **for all** expression traits  $T_i$  **do**
  - 3:     **for all** expression traits  $T_j, j \neq i$  **do**
  - 4:         **for all** genetic markers  $L_k$  **do**
  - 5:             Compute the Bayes factors for the triplet  $(L_k, T_i, T_j)$
  - 6:             Derive the posterior probability of the structure  $L_k \rightarrow T_i \rightarrow T_j$  given the data
  - 7:         **end for**
  - 8:         Save  $\max_k p(L_k \rightarrow T_i \rightarrow T_j)$  as the probability of gene  $i$  regulating gene  $j$
  - 9:     **end for**
  - 10: **end for**
  - 11: *Output:* Matrix of regulation probabilities
- 

(Algorithm 1). For BFCS, we used DMAGs to allow for the possibility of latent variables.

Rank	Gene	Chen et al.	trigger	BFCS	Rank	Gene	Chen et al.	trigger	BFCS
1	MDM35	0.973	0.999	0.678	1	FMP39	0.176	0.401	0.691
2	CBP6	0.968	0.997	0.683	2	DIA4	0.493	0.987	0.691
3	QRI5	0.960	0.985	0.678	3	MRP4	0.099	0.260	0.691
4	RSM18	0.959	0.984	0.672	4	MNP1	0.473	0.999	0.691
5	RSM7	0.953	0.977	0.684	5	MRPS18	0.527	0.974	0.690
6	MRPL11	0.924	0.999	0.670	6	MTG2	0.000	0.000	0.690
7	MRPL25	0.887	0.908	0.675	7	YNL184C	0.299	0.768	0.690
8	DLD2	0.871	0.896	0.660	8	YPL073C	0.535	0.993	0.690
9	YPRI26C	0.860	0.904	0.634	9	MBA1	0.290	0.591	0.690
10	MSS116	0.849	0.997	0.659	10	ACN9	0.578	0.927	0.690

(a) Genes regulated by NAM9, sorted by ‘Chen et al.’.     (b) Genes regulated by NAM9, sorted by ‘BFCS’.

Table 2: The column ‘Chen et al.’ shows the original results of the Trigger algorithm as reported in [1]. The ‘trigger’ column contains the probabilities we obtained when running the algorithm from the Bioconductor **trigger** package [14] on the entire yeast data set with default parameters. The column ‘BFCS’ contains the output of running Algorithm 1 on the yeast data set, for which we took a uniform prior over DMAGs.

In Table 2a, we report the top ten genes purported to be regulated by the putative regulator NAM9, sorted according to the probability estimates reported in [1]. We see that BFCS also assigns relatively high, albeit much more conservative, probabilities to the most significant regulatory relationships found by Trigger. In Table 2b, we see that some relationships ranked significant by BFCS are assigned a very small probability by Trigger. The regulatory relationship  $\text{NAM9} \rightarrow \text{MTG2}$ , of which both genes are associated with the mitochondrial ribosome assembly [15], is ranked sixth by BFCS, but is assigned zero probability by Trigger. This is because the genetic marker  $L_i$  exhibiting the strongest linkage with  $T_i$  (NAM9 in this case) is preselected in the Trigger algorithm and only the probability of  $L_i \rightarrow T_i \rightarrow T_j$  given the data is estimated, while other potentially more relevant genetic markers may be filtered out. With BFCS, on the other hand, we estimated the maximum probability of this structure for all



genetic markers (see also subsection 3.4).

In Subsection 3.3, we have computed an upper bound on the posterior probability  $p(L_k \rightarrow T_i \rightarrow T_j \mid \mathbf{D})$ , which is dependent on the chosen prior on causal structures and on the number of samples. For 112 observations (in the yeast data set) and a uniform prior on DMAGs with background knowledge (Table 1), we obtain a conservative upper bound of 0.6909. This explains why the BFCS probabilities are tightly packed together in the interval  $[0.690, 0.691]$  in Table 2b. If we use the prior probabilities derived from a uniform prior on DAGs with background knowledge, as in ‘BFCS DAG’, this upper bound increases to 0.7703 because there are fewer possible ‘full’ models competing against the ‘causal’ model. Whereas our posterior probability predictions are appropriately conservative for this number of observations, as reflected by the derived upper bound, Trigger often returns overconfident predictions.

## 5. Computational and time complexity

The simplicity and inherent parallelism of our approach makes it suitable for large-scale causal network inference. In this section, we evaluate the time and computational complexity of our algorithm and compare it against similar approaches. Assuming that the data correlation matrix required for deriving the Bayes factors in (6) has been precomputed, then the derivation takes constant time. Deriving the posterior probability of  $L_k \rightarrow T_i \rightarrow T_j$  from the Bayes factors also takes constant time, since we always have to look at a fixed number of eleven covariance structures. The computational complexity in Algorithm 1 is then driven by the nested iteration loop over all possible  $(L_k, T_i, T_j)$  triples in lines 2 to 4. Assuming that there are  $m$  genes in the regulatory network for which we have measured expression levels and  $l$  genetic markers, we arrive at a computational complexity of  $\mathcal{O}(lm^2)$ .

Any routine for deriving the posterior probability of  $L_k \rightarrow T_i \rightarrow T_j$  can be plugged inside the iteration loops in Algorithm 1. For instance, in the reference BGe procedure (Subsection 3.3), we replace lines 5 and 6 with a function that computes the BGe score of each causal structure on triplets. This involves summing up over a number of local scores for each node, where the complexity of each local computation depends on the number of nodes involved (the node and its parents). Since we are only computing the BGe score over triples, the computational complexity is also of order  $\mathcal{O}(1)$ . However, a single BGe score computation is typically more expensive than computing the Bayes factors, since the latter involves a number of simplifications.

The computation of the Bayes factors in (6) is amenable to vectorization. Instead of passing three correlation coefficients each time to the computation routine, we can pass three vectors of correlation coefficients and perform the computation element-wise. This way we can take advantage of processor architecture supporting SIMD (Single instruction, multiple data) instructions such as AVX [16]. Since in the vast majority of cases we will have the same number of observations for each triple of variables, we can make further savings by precomputing the prefactors  $f(n, \nu)$  and  $g(n, \nu)$  in (6).

In Figures 8 and 9 we illustrate the time complexity of the approaches discussed relative to the network size (number of variables) and to the number of data points. The time measurements were taken on an HP® EliteBook™ 850 G2 sporting an Intel® Core™ i7-5600U 2.60 GHz CPU with SSE4.1, SSE4.2 and AVX2 vectorization capabilities and 16GiB of SODIMM DDR3 Synchronous 1600 MHz RAM. To ensure a fair comparison, we did not include the time it takes Trigger to compute the local linkage between genetic markers and expression traits in the measurement. Figure 8 confirms our expectation that the run time for both BGe and BFCS increases cubically. We notice that BFCS outperforms the other two approaches and is extremely fast even for very large networks. Trigger scales better with the size of the network since it preselects the genetic marker with the strongest linkage for each expression trait pair, essentially reducing the computational complexity from  $\mathcal{O}(lm^2)$  to  $\mathcal{O}(m^2)$ . However, in Figure 9 we see that its execution time is strongly dependent on the amount of samples in the data set. This is because the Trigger algorithm involves computationally expensive operations that require permuting the data set in order to obtain generate null statistics for performing likelihood ratio tests.

## 6. Discussion

We have introduced a novel Bayesian approach for inferring gene regulatory networks that uses the information in the local covariance structure over triplets of variables to make statements about the presence of causal relationships. The probability estimates produced by BFCS constitute a measure of reliability in the inferred causal relations. One key advantage of our method is that we consider all possible causal structures at once, whereas other methods only look at and test for a subset of structures. Since we focus on discovering local causal structures, our method is simple, fast, and inherently parallel, which makes it applicable to very large data sets. Moreover, this enables us to consider more (and possibly better) candidates for estimating the probability of causal regulatory relationships given data than the more restricted search strategy employed by Trigger. We have demonstrated the effectiveness of our approach by comparing it against the Trigger algorithm, a state-of-the-art procedure for inferring causal regulatory relationships. Other methods for inferring gene regulatory networks such as ‘CIT’ [2] or ‘CMST’ [3] output  $p$ -values instead of probability estimates, which is why they are not directly comparable to BFCS.

In this paper, we have proposed simple uniform priors on two types of causal graph structures, namely DAGs and DMAGs. However, our method allows for more informative causal priors to be incorporated, taking into consideration properties such as the sparsity of the networks. Moreover, our approach is structure-agnostic, by which we mean we can consider different causal graph structures incorporating various data-generating assumptions. The tricky part is then to come up with an appropriate prior on the set of causal graph structures from which we assume the data is generated.

Our approach could be extended to other types of local structures in future work. A straightforward idea would be to consider more than three variables in

a local causal structure, which may allow us to discover causal links that cannot be found by looking only at triplets.

## Acknowledgments

This research has been partially financed by the Netherlands Organisation for Scientific Research (NWO), under project 617.001.451.

## Appendix A. Proofs

**Lemma 1** (Completeness of covariance structures). *There are only five possible canonical patterns for non-degenerate (full rank) covariance structures over three variables.*

*Proof.* We have three off-diagonal terms in the covariance matrix and three off-diagonal terms in the precision matrix that can be constrained to zero. This means that we have to consider  $2^6 = 64$  patterns of zeros. However, a constraint in the covariance matrix implies a constraint in the precision matrix and vice versa:

$$\Omega_{ij} = 0 \implies \Sigma_{ij}\Sigma_{kk} = \Sigma_{ik}\Sigma_{kj} \quad \wedge \quad \Sigma_{ij} = 0 \implies \Omega_{ij}\Omega_{kk} = \Omega_{ik}\Omega_{kj},$$

for any distinct  $i, j, k \in \{1, 2, 3\}$ . This leads to four implications, whereby if two terms are constrained to zero, (at least) two more have to be constrained to zero:

1.  $\begin{cases} \Omega_{ik} = 0 \\ \Omega_{jk} = 0 \end{cases} \implies \begin{cases} \Sigma_{jj}\Sigma_{ik} = \Sigma_{ij}\Sigma_{jk} \\ \Sigma_{ii}\Sigma_{jk} = \Sigma_{ij}\Sigma_{ik} \end{cases} \implies \begin{cases} \Sigma_{ik}(\Sigma_{ii}\Sigma_{jj} - \Sigma_{ij}^2) = 0 \\ \Sigma_{jk}(\Sigma_{ii}\Sigma_{jj} - \Sigma_{ij}^2) = 0 \end{cases} \xRightarrow{\Sigma, p.d.} \begin{cases} \Sigma_{ik} = 0 \\ \Sigma_{jk} = 0 \end{cases}$
2.  $\begin{cases} \Sigma_{ik} = 0 \\ \Sigma_{jk} = 0 \end{cases} \implies \begin{cases} \Omega_{jj}\Omega_{ik} = \Omega_{ij}\Omega_{jk} \\ \Omega_{ii}\Omega_{jk} = \Omega_{ij}\Omega_{ik} \end{cases} \implies \begin{cases} \Omega_{ik}(\Omega_{ii}\Omega_{jj} - \Omega_{ij}^2) = 0 \\ \Omega_{jk}(\Omega_{ii}\Omega_{jj} - \Omega_{ij}^2) = 0 \end{cases} \xRightarrow{\Omega, p.d.} \begin{cases} \Omega_{ik} = 0 \\ \Omega_{jk} = 0 \end{cases}$
3.  $\begin{cases} \Sigma_{ij} = 0 \\ \Omega_{ij} = 0 \end{cases} \implies \begin{cases} \Omega_{kk}\Omega_{ij} = \Omega_{ik}\Omega_{jk} = 0 \\ \Sigma_{kk}\Sigma_{ij} = \Sigma_{ik}\Sigma_{jk} = 0 \end{cases} \implies \begin{cases} \Omega_{ik} = 0 \vee \Omega_{jk} = 0 \\ \Sigma_{ik} = 0 \vee \Sigma_{jk} = 0 \end{cases}$
4.  $\begin{cases} \Sigma_{ik} = 0 \\ \Omega_{jk} = 0 \end{cases} \implies \begin{cases} \Omega_{jj}\Omega_{ik} = \Omega_{ij}\Omega_{jk} = 0 \\ \Sigma_{ii}\Sigma_{jk} = \Sigma_{ij}\Sigma_{ik} = 0 \end{cases} \xRightarrow{\Sigma, \Omega, p.d.} \begin{cases} \Omega_{ik} = 0 \\ \Sigma_{jk} = 0 \end{cases}$

Let  $z \in \{0, 1, 2, 3\}$  be the number of zeros in the covariance matrix. We explore the covariance structures in increasing order of  $z$ .

- $z = 0$  : 1) If there are also no zeros in the precision matrix, then we have a ‘full’ covariance structure. 2) If there is a zero in the precision matrix, then we have one of the three ‘causal’ covariance structures. 3) If there are two or more zeros in the precision matrix, then there are also zeros in the covariance matrix because of implication 1. This leads to a contradiction.
- $z = 1$  : 1) If there are no zeros in the precision, then we have one of the three ‘acausal’ covariance structures. 2) If there is at least one zero in the precision matrix, then via implication 3 or implication 4, we also have at least two zeros in the covariance matrix. This leads to a contradiction.
- $z = 2$  : Due to implication 2, we also have at least two zeros in the precision matrix. 1) If there are only these two zeros in the precision matrix, then we have one of three ‘independent’ covariance structures. 2) If all off-diagonal terms in the precision matrix are zero, then all three off-diagonal terms in the covariance matrix are zero (implication 1). This leads to a contradiction.
- $z = 3$  : In this case, the covariance is diagonal, in which case the precision is also diagonal. This means we have an ‘empty’ covariance structure.

In conclusion, we have determined that there are only eleven distinct covariance structures: one ‘full’, three ‘causal’, three ‘acausal’, three ‘independent’ and one ‘empty’.

Since a conditional independence for a trivariate multivariate Gaussian distribution is equivalent to either a zero in the correlation matrix or a zero in the inverse correlation matrix, we have to consider  $2^6 = 64$  different patterns. However, we shall see that due to overlap, these boil down to only the 11 conditional independence models: the potential zeroes in the correlation matrix give us  $2^3 = 8$  models, while the  $P_{12} = 0$ ,  $P_{13} = 0$ , and  $P_{23} = 0$ , constitute the other three models.

In our proof, we use the fact that the independence model induced by a multivariate Gaussian distribution is a compositional graphoid [9]. Between three variables, there are six possible (conditional) independences:  $X_1 \perp\!\!\!\perp X_2$ ,  $X_1 \perp\!\!\!\perp X_3$ ,  $X_2 \perp\!\!\!\perp X_3$ ,  $X_1 \perp\!\!\!\perp X_2 \mid X_3$ ,  $X_2 \perp\!\!\!\perp X_3 \mid X_1$ ,  $X_3 \perp\!\!\!\perp X_1 \mid X_2$ . If none of these independences hold, then we are in case 1.

If  $X_1 \perp\!\!\!\perp X_2$ , then we are in case  $\mathcal{M}_1$ , according to its definition. If in addition  $X_1 \perp\!\!\!\perp X_3$ , then  $X_1 \perp\!\!\!\perp (X_2, X_3)$  via the composition axiom, so we are in case  $\mathcal{M}_3$ . If in addition  $X_2 \perp\!\!\!\perp X_3$ , then  $X_2 \perp\!\!\!\perp (X_1, X_3)$  via the composition axiom, so we are also in case  $\mathcal{M}_3$ .

If one marginal independence holds, then we are in case 2, according to its definition. If two marginal independences hold, they must have one common variable, so we use the composition axiom to obtain that one variable is independent of the other two, hence we are in case 4. If all three marginal independences hold, then we are in case 5, because for example  $X_1 \perp\!\!\!\perp (X_2, X_3) \wedge X_2 \perp\!\!\!\perp X_3 \implies X_1 \perp\!\!\!\perp X_2 \perp\!\!\!\perp X_3$ .

If one conditional independence holds, then we are in case 3, according to its definition. If two conditional independences hold, we use the intersection axiom to obtain that one variable is independent of the other two, so we are again in case 4. If all three conditional independences hold, then the variables become mutually independent, so we are in case 5.

- $X_1 \perp\!\!\!\perp X_2 \iff R_{12} = 0$
- $X_1 \perp\!\!\!\perp X_3 \iff R_{13} = 0$
- $X_2 \perp\!\!\!\perp X_3 \iff R_{23} = 0$
- $X_1 \perp\!\!\!\perp X_2 \mid X_3 \iff P_{12} = 0 \iff R_{12} = R_{13}R_{23}$
- $X_1 \perp\!\!\!\perp X_3 \mid X_2 \iff P_{13} = 0 \iff R_{13} = R_{12}R_{23}$
- $X_2 \perp\!\!\!\perp X_3 \mid X_1 \iff P_{23} = 0 \iff R_{23} = R_{12}R_{13}$

□

## References

## References

- [1] L. S. Chen, F. Emmert-Streib, J. D. Storey, Harnessing Naturally Randomized Transcription to Infer Regulatory Relationships among Genes, *Genome Biology* 8 (10) (2007) R219.
- [2] J. Millstein, B. Zhang, J. Zhu, E. E. Schadt, Disentangling Molecular Relationships with a Causal Inference Test, *BMC Genetics* 10 (2009) 23.
- [3] E. C. Neto, A. T. Broman, M. P. Keller, A. D. Attie, B. Zhang, J. Zhu, B. S. Yandell, Modeling Causality for Pairs of Phenotypes in System Genetics, *Genetics* 193 (3) (2013) 1003–1013.
- [4] G. F. Cooper, A Simple Constraint-Based Algorithm for Efficiently Mining Observational Databases for Causal Relationships, *Data Mining and Knowledge Discovery* 1 (2) (1997) 203–224.
- [5] S. Mani, P. Spirtes, G. F. Cooper, A Theoretical Study of Y Structures for Causal Discovery, *UAI’06*, AUAI Press, Arlington, Virginia, United States, 2006, pp. 314–323.
- [6] N. Meinshausen, P. Bühlmann, High-Dimensional Graphs and Variable Selection with the Lasso, *The Annals of Statistics* 34 (3) (2006) 1436–1462.
- [7] T. Richardson, P. Spirtes, Ancestral Graph Markov Models, *The Annals of Statistics* 30 (4) (2002) 962–1030.
- [8] M. Studeny, *Probabilistic Conditional Independence Structures*, Springer Science & Business Media, 2006.
- [9] K. Sadeghi, S. Lauritzen, Markov properties for mixed graphs, *Bernoulli* 20 (2) (2014) 676–696. doi:10.3150/12-BEJ502.
- [10] T. Claassen, T. Heskes, A Logical Characterization of Constraint-based Causal Discovery, *UAI’11*, AUAI Press, Arlington, Virginia, United States, 2011, pp. 135–144.
- [11] J. Barnard, R. McCulloch, X.-L. Meng, Modeling Covariance Matrices in Terms of Standard Deviations and Correlations, with Application to Shrinkage, *Statistica Sinica* 10 (4) (2000) 1281–1311.
- [12] D. Geiger, D. Heckerman, *Learning Gaussian Networks*, *UAI’94*, Morgan Kaufmann Publishers Inc., San Francisco, CA, USA, 1994, pp. 235–243.
- [13] M. Kalisch, M. Mächler, D. Colombo, M. H. Maathuis, P. Bühlmann, Causal Inference Using Graphical Models with the R Package pcalg, *Journal of Statistical Software* 47 (1) (2012) 1–26. doi:10.18637/jss.v047.i11.

- [14] L. S. Chen, D. P. Sangurdekar, J. D. Storey, Trigger, Bioconductor, 2017. doi:10.18129/b9.bioc.trigger.
- [15] The UniProt Consortium, UniProt: A worldwide hub of protein knowledge, Nucleic Acids Research 47 (D1) (2018) D506–D515. doi:10.1093/nar/gky1049.
- [16] C. Lomont, Introduction to Intel® Advanced Vector Extensions (2011) 21.

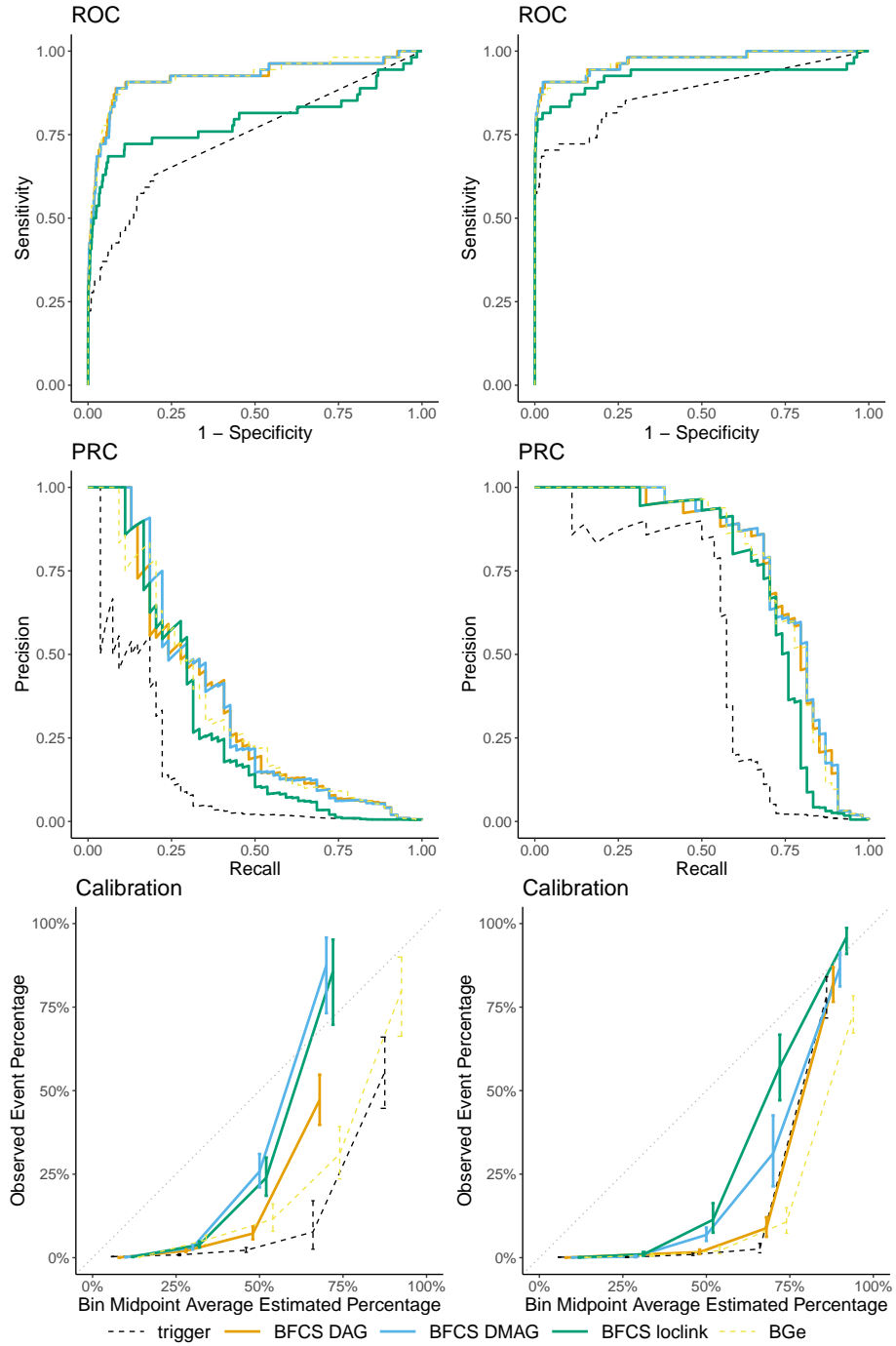


Figure 4: Evaluating the performance of detecting the 54 direct causal regulatory relationships in a (sparser) simulated GRN. We generated 100 samples (**left column**) and then 1000 samples (**right column**) from the network. We ran Trigger three times on the simulated data and averaged the results ('trigger') to account for differences when sampling the null statistics. We report the results of three BFCS versions, two like in Algorithm 1 where we take a uniform prior over DAGs ('BFCS DAG') and DMAGs ('BFCS DMAG'), respectively, and one in which we use the Trigger linkage search strategy ('BFCS loclink'). For reference, we also show the performance of an equivalent method that uses the BGe score ('BGe').



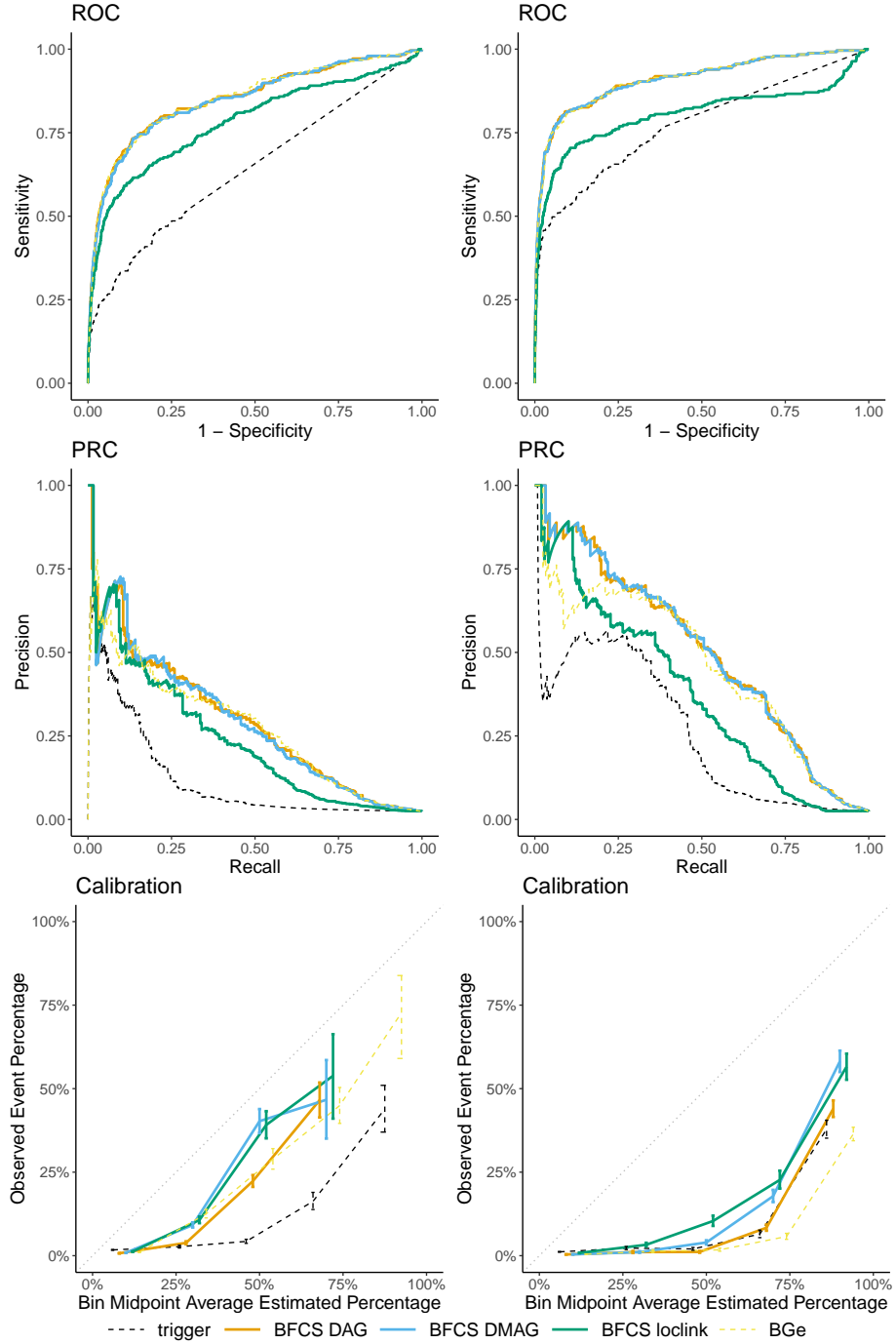


Figure 5: Evaluating the performance of detecting the 247 direct causal regulatory relationships in a (denser) simulated GRN. We generated 100 samples (**left column**) and then 1000 samples (**right column**) from the network. We ran Trigger three times on the simulated data and averaged the results (‘trigger’) to account for differences when sampling the null statistics. We report the results of three BFCS versions, two like in Algorithm 1 where we take a uniform prior over DAGs (‘BFCS DAG’) and DMAGs (‘BFCS DMAG’), respectively, and one in which we use the Trigger linkage search strategy (‘BFCS loclink’). For reference, we also show the performance of an equivalent method that uses the BGe score (‘BGe’).

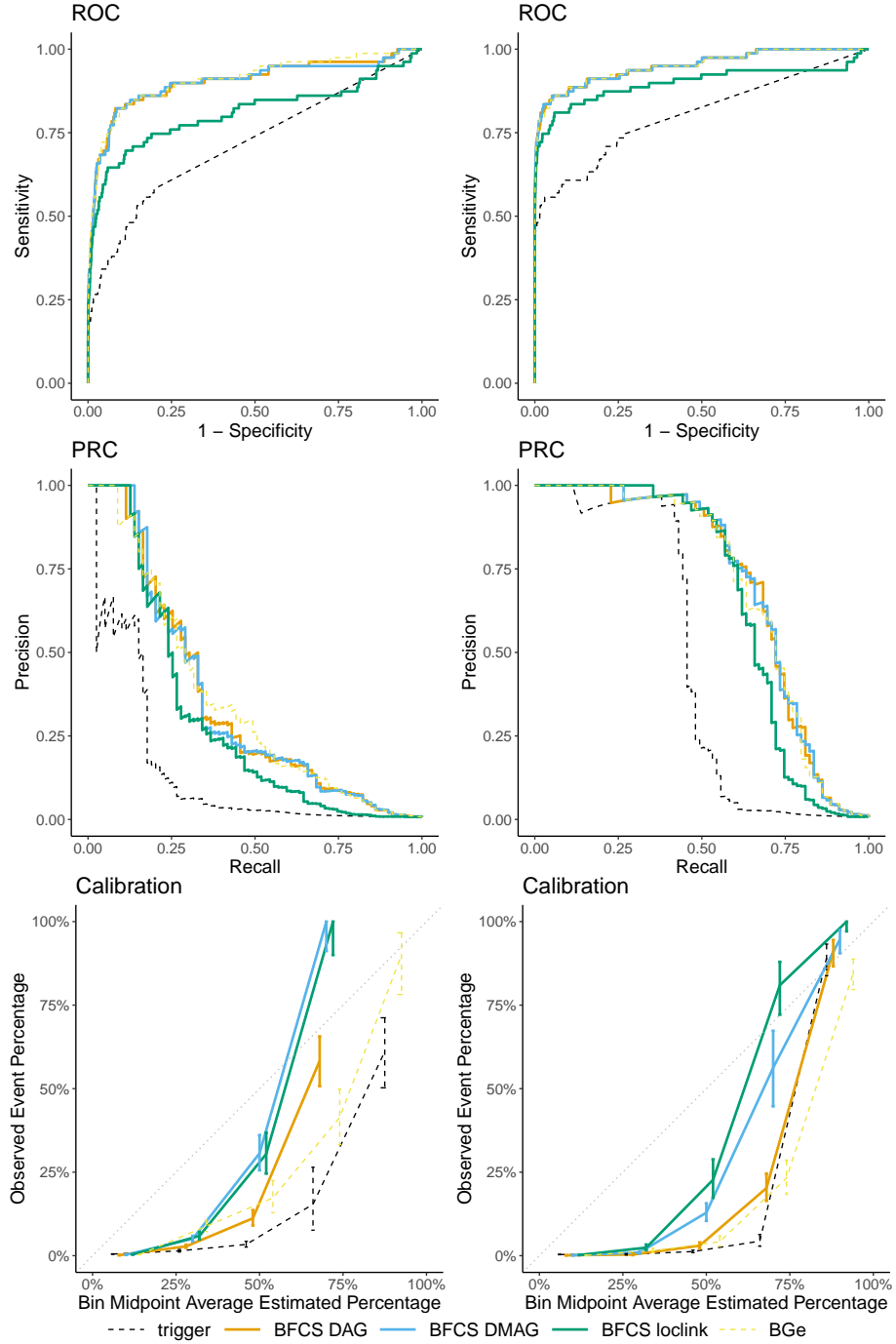


Figure 6: Evaluating the performance of detecting the 79 ancestral causal regulatory relationships in a (sparser) simulated GRN. We generated 100 samples (**left column**) and then 1000 samples (**right column**) from the network. We ran Trigger three times on the simulated data and averaged the results ('trigger') to account for differences when sampling the null statistics. We report the results of three BFCS versions, two like in Algorithm 1 where we take a uniform prior over DAGs ('BFCS DAG') and DMAGs ('BFCS DMAG'), respectively, and one in which we use the Trigger linkage search strategy ('BFCS loclink'). For reference, we also show the performance of an equivalent method that uses the BGe score ('BGe').

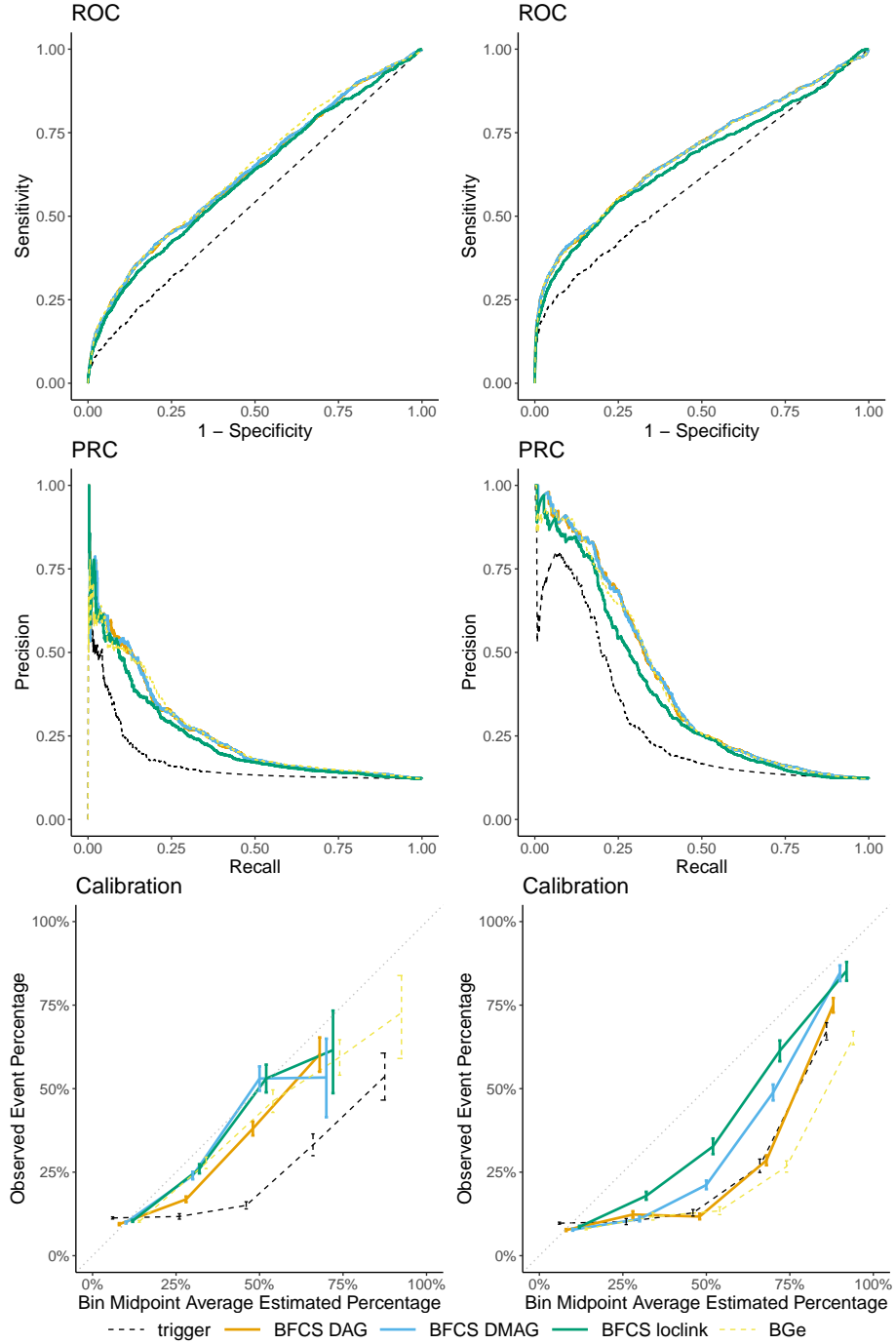


Figure 7: Evaluating the performance of detecting the 1211 ancestral causal regulatory relationships in a (denser) simulated GRN. We generated 100 samples (**left column**) and then 1000 samples (**right column**) from the network. We ran Trigger three times on the simulated data and averaged the results ('trigger') to account for differences when sampling the null statistics. We report the results of three BFCS versions, two like in Algorithm 1 where we take a uniform prior over DAGs ('BFCS DAG') and DMAGs ('BFCS DMAG'), respectively, and one in which we use the Trigger linkage search strategy ('BFCS loclink'). For reference, we also show the performance of an equivalent method that uses the BGe score ('BGe').

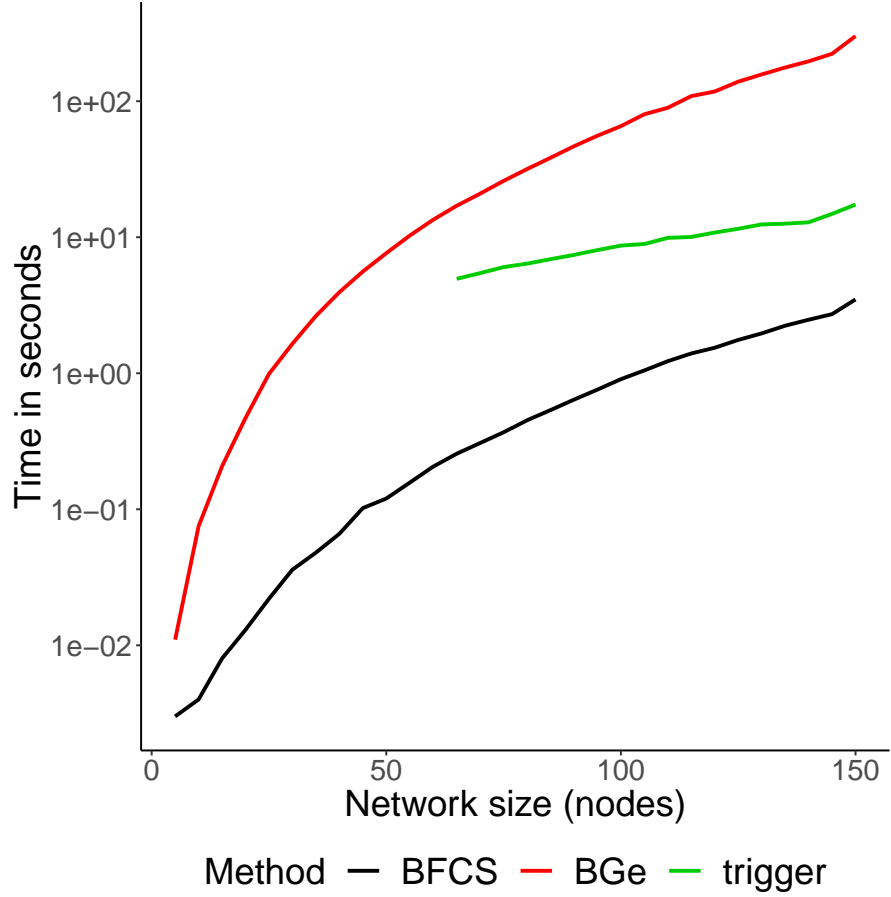


Figure 8: In this simulation, we generated GRNs of increasing size and measured the run time for each algorithm. The network size refers to the number of gene expression variables in our data set ( $m$ ). For each measurement, we simulated a GRN where the number of genetic markers ( $l$ ) is equal to the number of expression traits. We report the time measurements in base-10 logarithmic scale for BFCS, Trigger, and BGe versus the network size. For a number of nodes smaller than 75, we ran into problems while running Trigger having to do with the algorithm not being able to produce an estimate of  $\pi_0$ , the proportion of true null  $p$ -values. We have observed (not shown here) that the GRN density does not influence the time complexity.

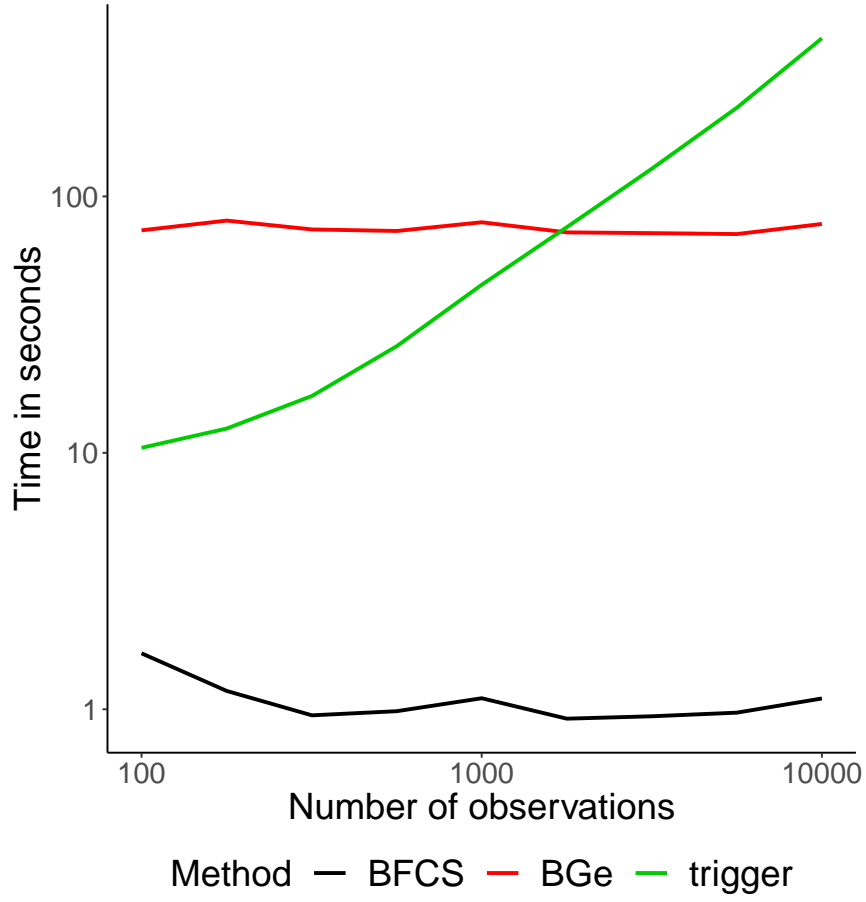


Figure 9: In this simulation, we generated GRNs with 100 expression traits and 100 genetic markers. At each step we increased the number of observations linearly on a logarithmic scale. We report the time measurements in base-10 logarithmic scale for BFCS, trigger, and BGe versus the number of observations in base-10 logarithmic scale. We see that the time complexity of Trigger is affected by the data sample size, unlike that of BFCS and BGe. For the last two algorithms we included the time it takes to compute the data correlation matrix.